Chemical Physics Letters, Volume 506, Issues 1-3, 11 April 2011, Pages 81-85

Accepted Manuscript

Filtering carbon dioxide through carbon nanotubes

Dimitrios Mantzalis, Nikolaos Asproulis, Dimitris Drikakis

PII: S0009-2614(11)00230-2
DOI: 10.1016/j.cplett.2011.02.054
Reference: CPLETT 29068

To appear in: *Chemical Physics Letters*

Received Date: 25 October 2010
Revised Date: 23 February 2011
Accepted Date: 24 February 2011

Please cite this article as: D. Mantzalis, N. Asproulis, D. Drikakis, Filtering carbon dioxide through carbon nanotubes, *Chemical Physics Letters* (2011), doi: 10.1016/j.cplett.2011.02.054

Filtering carbon dioxide through carbon nanotubes

Dimitrios Mantzalis, Nikolaos Asproulis, Dimitris Drikakis

Fluid Mechanics & Computational Science Department,
Cranfield University, United Kingdom

Abstract

Layering phenomena of carbon dioxide transported through carbon nanotubes are investigated through molecular dynamics simulations. The layering formation is examined for carbon nanotubes spanning from $(8, 8)$ to $(20, 20)$ subjected to pressures and temperatures that range from $1 - 20$ *bar* and $300 - 400$ K, respectively. Well defined layers are developed around the internal and external surface of the nanotubes for all the examined cases. It is shown that the number of layers along with their relative strength varies as a function of the nanotube's diameter, size, carbon dioxide density and gas-structure interactions.

Keywords: adsorption, carbon nanotubes, carbon dioxide, density layers, molecular dynamics

1. Introduction

Carbon dioxide is the most prominent greenhouse gas with more than 30 billion tons being released every year in the earth's atmosphere (1). More than 30% of the released CO_2 is produced from fossil fuel power plants (1, 2) and an almost equal portion from the continuously increasing number of vehicles. The increasingly high volumes of carbon dioxide emitted in the atmosphere have stimulated the interest of the scientific community towards the development of new strategies and techniques for carbon capture and sequestration. Technological advancements, arising from these innovative strategies, contribute to the implementation of CO_2 mitigation schemes with the expectation of a wide range of socio-economic benefits.

Carbon nanotubes (CNTs) are considered among the most promising nano-materials (3) encompassing a large application envelope that spans from nano-electronics and materials science (4, 5) to biology (6, 7). Over the last years, significant efforts have been devoted to exploring the capabilities of CNT technology in gas separation and filtration (8–11). Experimental studies and computational modelling have shown that gases can be transported inside single walled carbon nanotubes (SWCNTs) orders of magnitude faster compared to zeolites or other traditional microporous materials (12). Their very small pore size along with their almost frictionless graphitic walls offer a rare combination of high selectivity and transport efficiency (13) and make them ideal gas adsorbents (14). Although considerable efforts have been dedicated to investigating either CNT-based materials for hydrogen storage (15–18) or CNT behaviour in water environment (19–22), studies regarding interactions of CNT with CO_2 are scarce (12, 23, 24).

Although comparative studies of gas transport properties through CNTs are limited, it has been shown that carbon dioxide's adsorption rates are almost one order of magnitude higher compared to methane (25). CNTs show simultaneously hydrophobic and CO_2-phylic attributes causing carbon dioxide molecules to form layers in the vicinity of the graphitic walls whereas water molecules concentrate towards the centric axis of the tube. Carbon dioxide can bind in fewer adsorption sites compared to other gases such as H_2, O_2 and Ar indicating therefore a different adsorption mechanism (26).

The rapid transport of molecules through CNTs is primarily originated from the absence of any corrugation in the molecule-CNT potential energy surface (12). As a consequence, the slip length (27) observed inside the nanotubes are three to four orders of magnitude higher compared to their radius (28), indicating a nearly frictionless CNT interface. In the case of more hydrophobic solvents, the slip length values decrease due to the stronger interactions between the CNT walls and the gas molecules (29). Despite the experimental and computational efforts that have been dedicated over the last years, the transport of light gases through

carbon nanotubes along with the effects of the nanotube's characteristics are not entirely understood and cannot be described properly by Knudsen diffusion (30). In the present study molecular dynamics (MD) simulations, using the LAMMPS (31) simulation software, are employed to explore the intrinsic behaviour of carbon dioxide transport through one SWCNT, aiming to enhance our physical understanding regarding the layering phenomena observed close to the nanotube's graphitic walls.

2. Simulation Method

The computational domain consists of a cubic box with edges equal to 290 $\mathring{A}$ and periodic boundary conditions applied in all three directions. For the scope of the current study, different nanotubes are employed spanning from $(8, 8)$ to $(20, 20)$ under pressure and temperature conditions that range from $1 - 20$ bar and $300 - 400$ K respectively. For these conditions carbon dioxide remains gaseous avoiding any supercritical or liquid states (32). The volume outside the nanotube is filled with carbon dioxide molecules spanning from 442 to 13152, subject to the specific figures of pressure and temperature (33). The original CO_2 velocities are initialised based on a Gaussian distribution according to the temperature value of the corresponding case. The CO_2 molecules are represented by utilising a spherical model (34, 35) with the parameters for the van der Waals interactions being $\varepsilon_{CO_2}/k_B = 235.9$ K and $\sigma_{CO_2} = 3.454$ $\mathring{A}$ and mass equal to 44.010 g/mol. Previous computational studies (19, 23) show that the use of a spherical model for simulating the CO_2 and its interactions with the SWCNTs provides reasonable approximation compared to linear models for pressures up to 100 bar.

Although the structural properties of the nanotubes, like flexibility, may affect the transport behaviour of the molecules inside and around the nanotubes, in the current study the CNTs are assumed to be rigid with parameters $\varepsilon_{C^*}/k_B = 28.0068$ K and $\sigma_{C^*} = 3.4$ $\mathring{A}$ (19), where C^* corresponds to CNTs' carbon atom. This assumption is consistent with previous theoretical and numerical studies (36). The NVT ensemble (isochoric-isothermic) (37) is employed in the simulations with time step $\delta t = 1fs$; $2 \cdot 10^4$ time steps have been performed for equilibration corresponding to 20 ps and another $2 \cdot 10^7$ time steps for averaging corresponding to 20 ns.

3. Results and Discussion

3.1. Layering Phenomena

Fig. 1 shows the formation of carbon dioxide layers inside and around the nanotubes at temperature 300 K and pressure 20 bar. The internal volume of the nanotube is divided to axial bins with characteristic structures being formed in the vicinity of the carbon surface, thus resulting in strong density layering independently of the nanotube's size. The number of the inner layers formed (Fig. 2(a)) varies and is not always an increasing function of the tube's diameter, as it has been reported in previous studies of oxygen transport in CNTs (38). The formation of the layers is generated due to the combined effect of the nanotube's radius, the gas-structure interactions and the van der Waals bond length between the gas molecules. A characteristic prime internal layer is developed, for all the examined cases (as seen in Fig. 2), at a certain distance from the tube's wall which is comparable to the zero-crossing distance $\sigma_{CO_2-C^*}$. The development of the internal prime layer reduces the volume that is available to the carbon dioxide molecules to travel within the nanotube. The effects of the available volume reduction are stronger in cases where the radius of the nanotube is comparable to the characteristic distance of the prime layer from the tube's wall, causing in some cases the formation of either triple or (fairly strong) secondary layers.

In the $(8, 8)$ nanotube, only the prime internal layer is observed. Due to its small internal volume and its large surface-to-volume ratio, the fluid-structure interactions dominate, thus causing the carbon dioxide particles to remain in a layer structure around the graphitic walls. As the radius increases further, multi-layer formations, either double or triple, are observed. The additional layers are developed at a distance from the prime one, comparable to the relaxation distance $\sigma_{CO_2-CO_2}$. The secondary layer appears initially in the $(10, 10)$ nanotube and remains for the rest of the examined cases, where larger diameters are employed. Apart from the $(10, 10)$ nanotube, the secondary density layer is less strong compared to the prime one since

the interactions from the graphitic walls diminish for the gas molecules that lie further inside the tube. For the $(10, 10)$ nanotube the secondary layer is formed exactly at the centre of tube. The repulsive forces from the tube's walls and the CO_2 molecules of the prime layer combined with the small volumes of the axial slabs involved, cause the remaining carbon dioxide molecules to stay at the centre of the nanotube axis at high densities (Fig. 2(a)). The latter leads to capillary condensation issues, which require further attention and will be examined in future studies.

The development of triple layering is observed only in the $(16, 16)$ nanotube. The third layer lies at the nanotube's axis and is formed due to the combined effect of the tube's size and gas interaction parameters. Equivalent to the formation of the secondary layer to the $(10, 10)$ nanotube, the CO_2 molecules that remain in the two outer layers along with the graphitic walls push the rest of the carbon dioxide particles towards the centric axis of the cylinder. Due to the lack of available motion space the remaining CO_2 molecules generate this third layering structure. Generally, it can be noticed that as the interior volume increases, the surface-to-volume ratio decreases thereby resulting in lower density values both at the prime and secondary density peaks. However, in all the examined scenarios the carbon dioxide density inside the SWCNT remains at around an order of magnitude higher compared to the bulk one.

Fig. 2(b) shows the characteristic structures developed at the external space of the nanotubes. These layering structures are primarily affected by the size of the contact surface between the SWCNT and the carbon dioxide molecules. For all the examined cases, two layers are identified; a major one in the proximity of SWCNT at a certain distance from the tube's walls and a secondary one similarly placed at a specific distance from the main layer. As the diameter of the nanotubes increases, their external surface increases linearly thus attracting a larger number of CO_2 molecules, which is translated to an increase of the main layer's density values (Fig. 2(b)). The external surfaces of the nanotubes are exposed to the CO_2 in a more direct way than the internal ones, where the adsorption process is initiated at the ends of the tube, followed by diffusion to the nanotube's interior. As a result, adsorption on external surfaces reaches equilibrium much faster than on the interior, under the same pressure and temperature conditions (39).

Fig. 3(a) shows the radial density profiles as function of pressure at 300 K in the internal space of a $(20, 20)$ nanotube. The pressure does not impact the layers' topology, which remains intact as previously described, however, it affects the peak values of the prime density layers along with the development of the secondary ones. Specifically, as the pressure increases, the formation of secondary layers is fostered and the prime density maxima, as absolute values, are enhanced (see Fig. 3(a)). Although the prime density layers become stronger when pressure increases, their strength relative to the bulk density of the fluid is a decreased function of pressure, as shown in Fig. 3(b). Higher pressure values imply higher densities, however, the density layering is not increasing proportionally to the increment of the medium's bulk density, thus resulting in a declining trend of the normalised maxima. Despite the considerable difference between the prime peak values for $P = 1$ bar and $P = 5$ bar (Fig. 3(a)), the normalised density profiles (Fig. 3(b)) show that density strength remains almost the same and about three orders of magnitude higher than the bulk figure. As the pressure further increases, the non-normalised profiles show that the density tends non-linearly to a maximum value corresponding to the maximum number of carbon dioxide molecules that can be accommodated around the graphitic walls of the nanotube. Hence, the relative adsorption performance is a diminishing function of pressure and, if the pressure values continue to grow, the saturation effects will be dominant and this decreasing behaviour will be more evident. Fig. 3(a) and Fig. 3(b) show the external normalised and non-normalised density profiles for the $(20, 20)$ nanotube at $T = 300$ K. Comparing the external and the internal normalised densities, is apparent that low pressures affects the adsorption by the external surface of the nanotube to a higher degree than the internal one.

3.2. Adsorption Isotherms

Fig. 4(a) presents the adsorption isotherms of CO_2 in four arm chair (n, n) nanotubes at 300 K. The total adsorption for each case has been normalised over the maximum adsorption of the $(8, 8)$ nanotube ($P = 20$ bar, $T = 300$ K), aiming to provide a more quantitative understanding of its dependency from the nanotube's size. The total adsorption calculations are based on the number of molecules that have been adsorbed both on the internal and external surface of the nanotubes. For the external molecules, we consider

that the adsorbed ones are those that belong to the first density layer formed in the vicinity of the SWCNT, and more specifically at a distance less than 5 $\AA$ from the tube walls (see Fig. 2(b)).

At low pressures, adsorption does not have a clear dependence on the tube size as can be observed by the small total adsorption deviations among the examined nanotubes (see Fig. 4(a)). Lower values of pressure are related to lower densities and, consequently, to smaller number of CO_2 molecules that travel through the nanotube leading to restricted capacity rates. However, as the pressure increases above 10 *bar* the density values become sufficient to reveal the importance of the nanotube's surface and volume. At higher pressures, larger nanotubes present greater CO_2 capture rates since the uptake is not restricted by the number of CO_2 molecules but from available SWCNT's volumes. At 20 *bar*, it is clear that nanotubes with larger diameters show greater capacity due to (i) their larger interior volume that can accommodate a larger number of CO_2 molecules; and (ii) their larger surface that generates stronger external density layers and, consequently, increases the carbon dioxide molecules adsorbed on the external surface. Another element that is observed is that each adsorption isotherm consists of two phases, a linear and an asymptotic one, with the latter corresponding to the beginning of the saturation process. The asymptotic phase is related to saturation effects that take place as the density of the medium increases due to the increased pressure. As the nanotube's radius increases, the transition to the asymptotic phase is delayed since nanotubes with larger internal volume and external surface require larger amount of carbon dioxide molecules to become saturated.

Fig. 4(b) shows the adsorption isobars for the examined nanotubes, showing the changes in their adsorption capacity as a function of temperature at constant pressure of 20 *bar*. At 300 K the $(20, 20)$ nanotube presents more than 25% higher adsorption rates compared to the $(8, 8)$ one. However, as the temperature increases these differences become smaller, with the adsorption capacity of the $(20, 20)$ and $(8, 8)$ approaching the capacity values of the other nanotubes. As temperature rises, the secondary layers, both internal and external, diffuse almost instantly followed by the prime internal layer and last by the prime external layer which is the one with the smaller diffusion rates. The density reduction in the internal and external layers is reflected to a subsequent reduction of total adsorption as higher values of temperature are employed (Fig. 4(b)). It appears that as the kinetic energy increases, due to the increased temperature, the CO_2 molecules show higher diffusivities preventing them from staying adsorbed in the nanotube (30).

4. Concluding Overview

In conclusion, the present study shows a well defined pattern of CO_2 layer formation, which is dependent on the tube's size, and gas-structure interactions. The formation of carbon dioxide layers in the vicinity of the tube's graphitic walls have been examined for pressure and temperature ranging from $1 - 20$ *bar* and $300 - 400$ K respectively. The numerical experiments showed that, apart from the primary layers formed around the CNTs, secondary and even tertiary density layers are observed in the internal volume of the tube. Specifically, if the tube's radius is almost double or triple the equilibrium distance between the internal layers then their strength is enhanced, as shown for the $(10, 10)$ and $(16, 16)$ SWCNTs. The variation of the density behaviour as a function of the nanotubes diameter leads to the conclusion that care must be exercised in choosing nanotubes with the appropriate characteristics that correspond to optimum operating conditions for real-life applications.

References

[1] D. Aaron, C. Tsouris, Separation Science and Technology 40 (2005) 321–348.
[2] I. C. Karagiannis, P. G. Soldatos, Energy Policy 38 (2010) 3891–3897.
[3] R. H. Baughman, A. A. Zakhidov, W. A. De Heer, Science 297 (2002) 787–792.
[4] K. Kato, M. Kitajima, Journal of the Vacuum Society of Japan 53 (2010) 317–326.
[5] A. Star, Y. Lu, K. Bradley, G. Grner, Nano Letters 4 (2004) 1587–1591.
[6] S. Kim, Z. Kuang, J. Grote, B. Farmer, R. Naik, Nano Letters 8 (2008) 4415–4420.
[7] A. Zheng, M.and Jagota, E. Semke, B. Diner, S. McLean, R.S.and Lustig, R. Richardson, N. Tassi, Nature Materials 2 (2003) 338–342.
[8] J. Kong, N. R. Franklin, C. Zhou, M. G. Chapline, S. Peng, K. Cho, H. Dai, Science 287 (2000) 622–625.

[9] P. Bernardo, E. Drioli, G. Golemme, Industrial and Engineering Chemistry Research 48 (2009) 4638–4663.
[10] H.-H. Tseng, I. Kumar, T.-H. Weng, C.-Y. Lu, M.-Y. Wey, Desalination 240 (2009) 40–45.
[11] J. Pitakarnnop, S. Varoutis, D. Valougeorgis, S. Geoffroy, L. Baldas, S. Colin, Microfluidics and Nanofluidics 8 (2010) 57–72.
[12] A. I. Skoulidas, D. M. Ackerman, J. K. Johnson, D. S. Sholl, Physical Review Letters 89 (2002) 185901.
[13] A. Noy, H. G. Park, F. Fornasiero, J. K. Holt, C. P. Grigoropoulos, O. Bakajin, Nano Today 2 (2007) 22–29.
[14] W. Shi, J. K. Johnson, Physical Review Letters 91 (2003) 015504.
[15] G. Mpourmpakis, G. E. Froudakis, G. P. Lithoxoos, J. Samios, Nano Letters 6 (2006) 1581–1583.
[16] G. Mpourmpakis, E. Tylianakis, G. E. Froudakis, Nano Letters 7 (2007) 1893–1897.
[17] J. Zhao, A. Buldum, J. Han, J. Lu, Nanotechnology 13 (2002) 195–200.
[18] A. C. Dillon, K. M. Jones, T. A. Bekkedahl, C. H. Kiang, D. S. Bethune, M. J. Heben, Nature 386 (1997) 377–379.
[19] A. Alexiadis, S. Kassinos, Chemical Physics Letters 460 (2008) 512–516.
[20] Y. Qiao, G. Cao, X. Chen, Journal of the American Chemical Society 129 (2007) 2355–2359.
[21] E. Kotsalis, J. Walther, P. Koumoutsakos, International Journal of Multiphase Flow 30 (2004) 995–1010.
[22] J. S. Pushparajalingam, M. Kalweit, M. Labois, D. Drikakis, Journal of Computational and Theoretical Nanoscience 6 (2009) 2156–2163.
[23] A. Skoulidas, D. Sholl, J. Johnson, Journal of Chemical Physics 124 (2006) 1–7.
[24] C. Matranga, L. Chen, M. Smith, E. Bittner, J. Johnson, B. Bockrath, Journal of Physical Chemistry B 107 (2003) 12930–12941.
[25] L. Huang, L. Zhang, Q. Shao, L. Lu, X. Lu, S. Jiang, W. Shen, Journal of Physical Chemistry C 111 (2007) 11912–11920.
[26] M. Bienfait, P. Zeppenfeld, N. Dupont-Pavlovsky, M. Muris, M. R. Johnson, T. Wilson, M. DePies, O. E. Vilches, Physical Review B - Condensed Matter and Materials Physics 70 (2004) 035410.
[27] N. Asproulis, D. Drikakis, Physical Review E - Statistical, Nonlinear, and Soft Matter Physics 81 (2010) 061503.
[28] B. J. Hinds, N. Chopra, T. Rantell, R. Andrews, V. Gavalas, L. G. Bachas, Science 303 (2004) 62–65.
[29] M. Majumder, N. Chopra, R. Andrews, B. J. Hinds, Nature 438 (2005) 44.
[30] A. Skoulidas, D. Sholl, J. Johnson, Journal of Chemical Physics 124 (2006) 1–7.
[31] S. Plimpton, Journal of Computational Physics 117 (1995) 1–19.
[32] E. Beckman, Journal of Supercritical Fluids 28 (2004) 121–191.
[33] P. Linstrom, E. W.G. Mallard, NIST Chemistry WebBook, NIST Standard Reference Database Number 69, 2010.
[34] A. Vishnyakov, P. Ravikovitch, A. Neimark, Langmuir 15 (1999) 8736–8742.
[35] P. I. Ravikovitch, A. Vishnyakov, R. Russo, A. V. Neimark, Langmuir 16 (2000) 2311–2320.
[36] X. Chen, G. Cao, A. Han, V. K. Punyamurtula, L. Liu, P. J. Culligan, T. Kim, Y. Qiao, Nano Letters 8 (2008) 2988–2992.
[37] M. Allen, D. Tildesley, Computer Simulation of Liquids, 1987.
[38] K. H. Lee, S. B. Sinnott, Nano Letters 5 (2005) 793–798.
[39] D. S. Rawat, V. Krungleviciute, L. Heroux, M. Bulut, M. M. Calbi, A. D. Migone, Langmuir 24 (2008) 13465–13469.

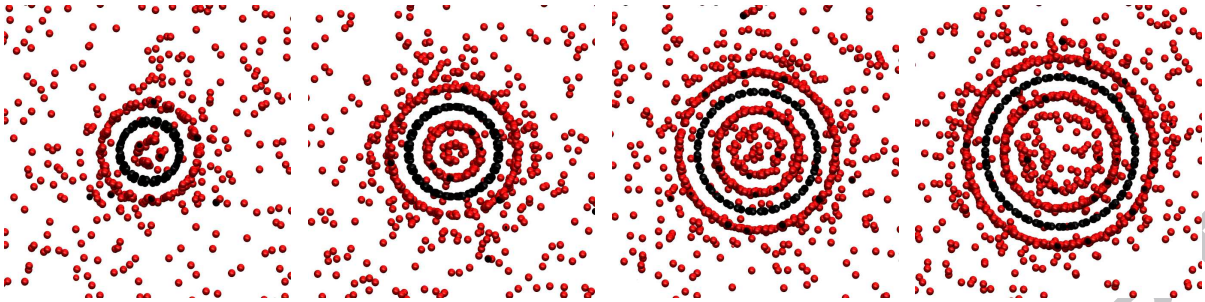

(a) $(8,8)$ (b) $(12,12)$ (c) $(16,16)$ (d) $(20,20)$

Figure 1: Projections of CO_2 distributions in $(8,8)$,$(12,12)$,$(16,16)$ and $(20,20)$ nanotubes at $T = 300\ K$ and $P = 20\ bar$

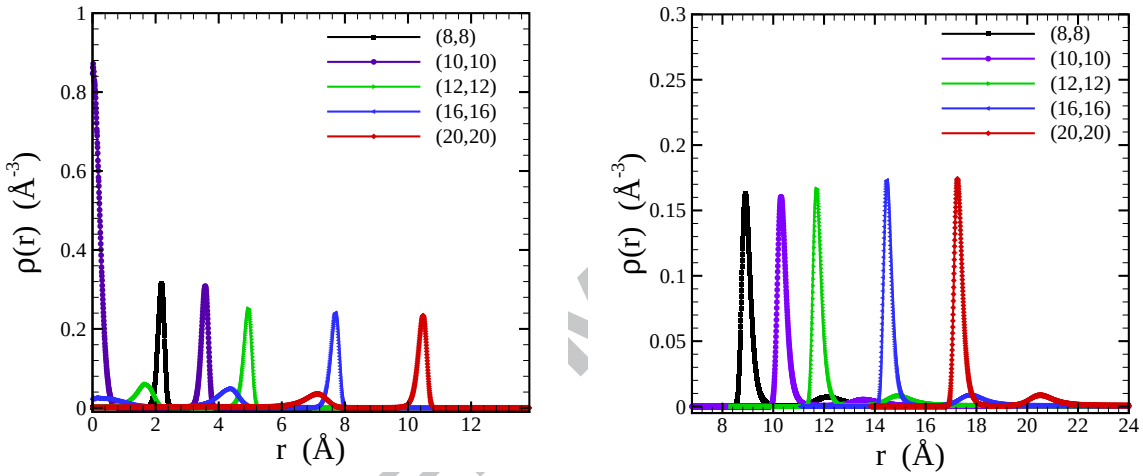

(a) Internal density profiles (b) External density profiles

Figure 2: Density profiles versus central distance (r) from the centre of the nanotube for various nanotubes at $T = 300\ K$ and $P = 20\ bar$

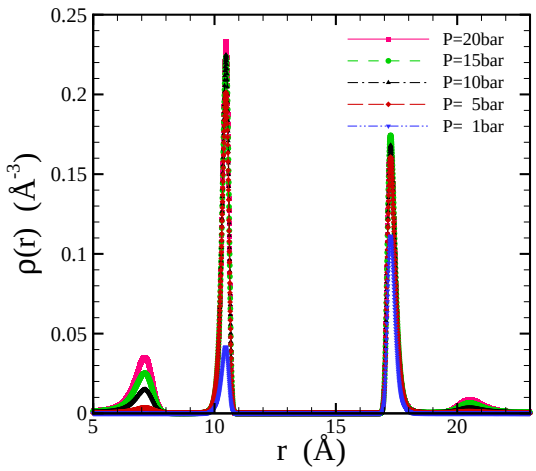

(a) Density profiles for $(20, 20)$

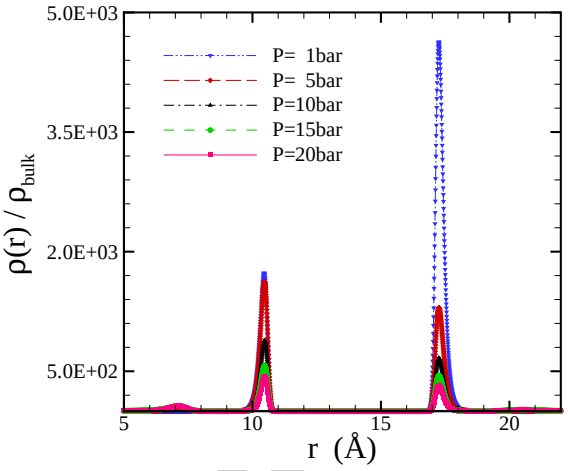

(b) Normalised density profiles for $(20, 20)$

Figure 3: Internal and external density profiles versus central distance (r) from the centre of the nanotube for a $(20, 20)$ nanotube at $T = 300\ K$ and various pressures

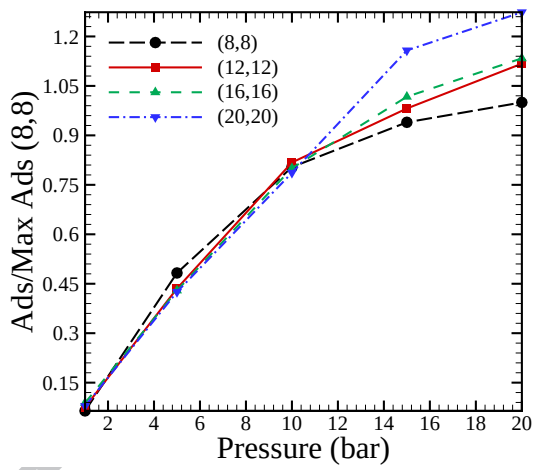

(a) Isotherms at $T = 300\ K$

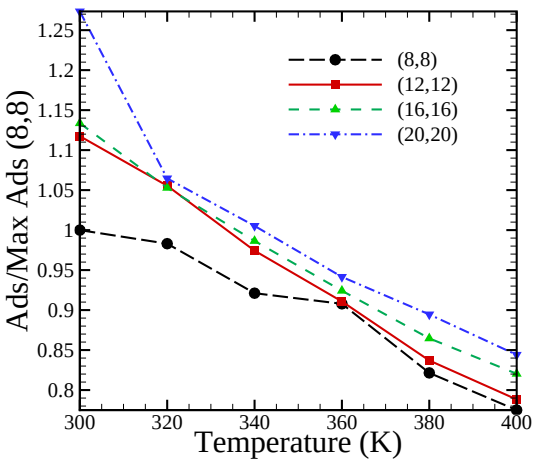

(b) Isobars at $P = 20\ bar$

Figure 4: Adsorption isotherms and isobars for various nanotubes normalised by the case of $(8, 8)$ nanotube at $P = 20\ bar$ and $T = 300\ K$

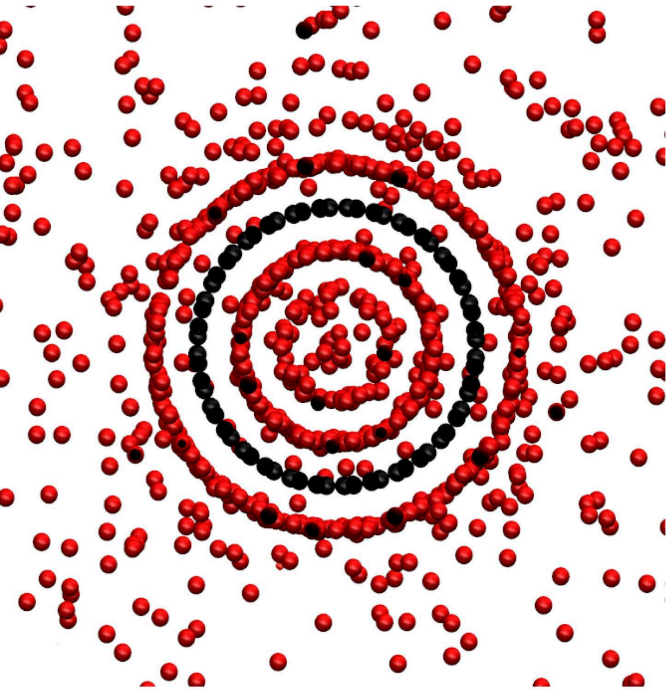

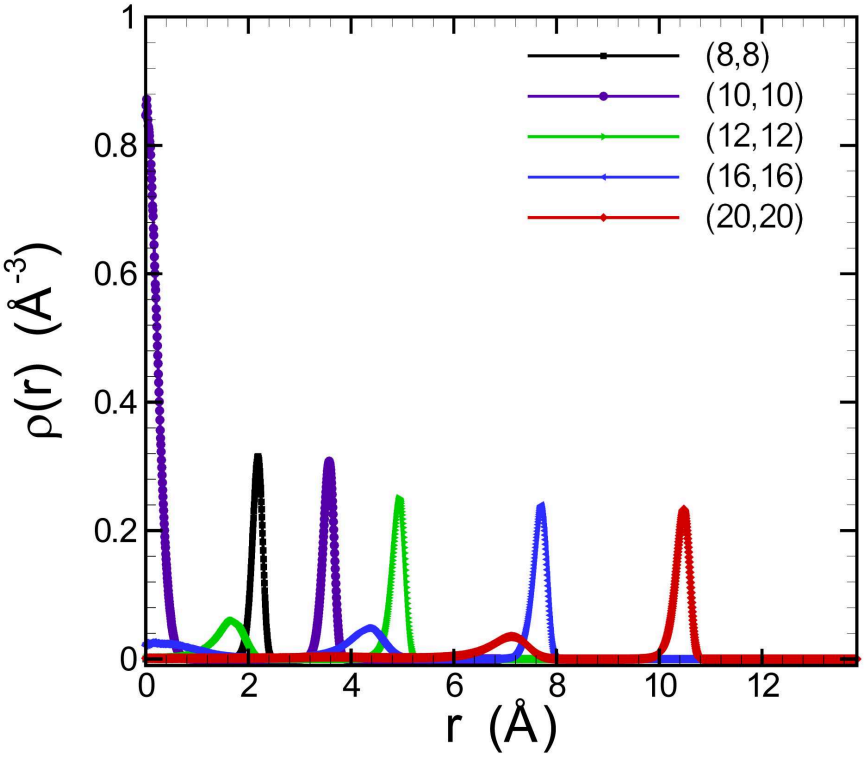

- The objective of the current work is to study the layering formation in the vicinity of single walled carbon nanotubes through molecular dynamics simulations in order to obtain physical insights regarding the filtering capability of CNTs
- Apart from the primary layers formed around the CNTs, secondary and even tertiary density layers are observed in the internal volume of the tube.
- The formation of the additional layers is dependent on the tube's size, chirality and gas-structure interactions and follows a well defined pattern.
- Low pressures affect to a higher degree the adsorption undergone by the external surface of the nanotube compared to the internal one.
- As the pressure increase the adsorption as absolute value increases initially linearly and then followed by an asymptotic profile.
- The strength of the density layers normalised to the bulk density decreases as pressure increases.

Filtering carbon dioxide through carbon nanotubes

Mantzalis, Dimitrios

2011-04-11T00:00:00Z

Dimitrios Mantzalis, Nikolaos Asproulis and Dimitris Drikakis. Filtering carbon dioxide through carbon nanotubes. Chemical Physics Letters, Volume 506, Issues 1-3, 11 April 2011, Pages 81-85
http://dx.doi.org/10.1016/j.cplett.2011.02.054